NMR IN BIOMEDICINE
NMR Biomed. 1999;**12**:145–156

On the inhibition of hepatic glycogenolysis by fructose. A ^{31}P-NMR study in perfused rat liver using the fructose analogue 2,5-anhydro-D-mannitol

K. Bruynseels,[1] N. Bergans,[1] N. Gillis,[1] F. van Dorpen,[1]† P. Van Hecke,[1] W. Stalmans[2] and F. Vanstapel[1]*

[1]Biomedical NMR Unit, Department of Radiology, B-3000 Leuven, Belgium
[2]Department of Biochemistry, Faculteit Geneeskunde, Katholieke Universiteit Leuven, Belgium

Received 7 April 1998; revised 8 July 1998; accepted 8 July 1998

ABSTRACT: Inhibition of hormone-stimulated hepatic glycogenolysis by fructose (Fru) has been attributed to accumulation of the competitive inhibitor Fru1*P* and/or to the associated depletion of the substrate phosphate (P_i). To evaluate the relative importance of either factor, we used the Fru analogue 2,5-anhydro-D-mannitol (aHMol). This analogue is avidly phosphorylated, traps P_i, and inhibits hormone-stimulated glycogenolysis, but it is not a gluconeogenic substrate, and hence does not confound glycogenolytic glucose production. Livers were continuously perfused with dibutyryl-*c*AMP (100 μM) to clamp phosphorylase in its fully activated *a* form. We administered aHMol (3.8 mM), and studied changes in glycogenolysis (glucose, lactate and pyruvate output) and in cytosolic P_i and phosphomonoester (PME), using *in situ* ^{31}P-NMR spectroscopy ($n = 4$). Lobes of seven livers perfused outside the magnet were extracted for evaluation, by high-resolution ^{31}P-NMR, of the evolution of aHMol1*P* and of aHMol(1,6)P_2. After addition of aHMol, both glycogenolysis and the NMR P_i signal dropped precipitously, while the PME signal rose continuously and was almost entirely composed of aHMol1*P*. Inhibition of glycogenolysis in excess of the drop in P_i could be explained by continuing accumulation of aHMol1*P*. A subsequent block of mitochondrial ATP synthesis by KCN (1 mM) caused a rapid increase of P_i. Despite recovery of P_i to values exceeding control levels, glycogenolysis only recovered partially, attesting to the P_i-dependence of glycogenolysis, but also to inhibition by aHMol phosphorylation products. However, KCN resulted in conversion of the major part of aHMol1*P* into aHMol(1,6)P_2. Residual inhibition of glycogenolysis was due to aHMol1*P*. Indeed, the subsequent withdrawal of aHMol caused a further gradual decrease in the proportion of aHMol1*P* (being converted into aHMol(1,6)P_2, in the absence of *de novo* aHMol1*P* synthesis), and this resulted in a gradual de-inhibition of glycogenolysis, in the absence of marked changes in P_i. Glycogenolytic rates were consistently predicted by a model assuming non-saturated P_i kinetics and competition by aHMol1*P* exclusively: In conclusion, limited P_i availability and the presence of competitive inhibitors are decisive factors in the control of the *in situ* catalytic potential of phosphorylase *a*.

KEYWORDS: phosphate; metabolite trapping; metabolic regulation; cyanide; glycogenesis

INTRODUCTION

The liver is the major site for disposal of fructose (Fru). Its hepatic metabolism has been well documented.[1–4] Avid phosphorylation by fructokinase results in accumulation of Fru1*P* which joins the glycolytic/gluconeogenic path through hepatic phosphofructoaldolase and triokinase. The accumulation of Fru1*P* coincides with a drop in P_i and ATP. These effects can be monitored by ^{31}P-NMR.[5]

Fru promotes deposition of glycogen. The mechanism appears to be hormone-independent,[6] and has been attributed to changes in metabolites inhibiting the glycogen-degradative path, while directing substrate flow toward glycogen synthesis.[2,7] Fru prevents hormone-stimulated glycogenolysis.[8–10] The marked inhibition of

**Correspondence to:* F. Vanstapel, Biomedical NMR Unit, Campus Gasthuisberg O/N 08, Herestraat 49, B-3000 Leuven, Belgium.
E-mail: Florent.Vanstapel@med.kuleuven.ac.be
Contract/grant sponsor: Fund for Medical Scientific Research (Belgium); *contract grant number:* 3.0064.94.
Contract/grant sponsor: Research Council of the Katholieke Universiteit Leuven; *contract grant number:* OT/93/31.
Contract/grant sponsor: Fund for Scientific Research–Flanders (Belgium); *contract grant number:* G.0360.98.

Abbreviations used: aHMol, 2,5-anhydro-D-mannitol; aHMol1*P*, 2,5-anhydro-D-mannitol 1-phosphate; aHMol(1,6)P_2, 2,5-anhydro-D-mannitol 1,6-bisphosphate; aHMol*P*, "total" 2,5-anhydro-D-mannitol phosphate ester; Bt_2*c*AMP, N^6,$O^{2'}$-dibutyryl adenosine 3′:5′-monophosphate; Fru, D-fructose; Fru1*P*, D-fructose 1-phosphate; NTP, nucleoside triphosphate (mainly ATP); P_i, *O*-phosphate; PDE, phosphodiester; PME, phosphomonoester.

Enzymes:EC 2.4.1.1,α-1,4-glucan:*o*-phosphate glucosyltransferase (glycogen phosphorylase);EC 2.7.1.1,ATP:D-hexose 6-phosphotransferase (hexokinase);EC 2.7.1.4,ATP:D-ketohexose 1-phosphotransferase (fructokinase);EC 2.7.1.11,ATP:D-fructofuranose-6-phosphate 1-phosphotransferase (phosphofructokinase);EC 4.1.2.13,D-fructose-1,6-bisphosphate D-glyceraldehyde-3-phosphate lyase (phosphofructoaldolase).

 CCC 0952–3480/99/030145–12 $17.50

maximal hormone-stimulated glycogenolysis by Fru has been related to direct inhibition of the catalytic efficiency of phosphorylase *a*, secondary to accumulation of Fru1*P*,[11–12] to the concomitant depletion of the substrate, P_i,[10] or to both mechanisms acting simultaneously.[8,13–14] A quantitative evaluation of the *in situ* effectiveness of either factor in the inhibition of phosphorylase *a* has been difficult to establish.[1] Gluconeogenesis from Fru compounds the evaluation of hepatic glucose production as an index of glycogenolysis.[14] Furthermore, an evaluation of the net loss of tissue glycogen as a function of tissue P_i and of Fru1*P* levels, chemically determined on tissue extracts, is compounded by the fact that these methods may overestimate true cytosolic P_i levels, as assessed by ^{31}P-NMR.[15–16]

Metabolic effects of Fru are mimicked by other phosphorylatable substrates (e.g. glycerol),[1] many of which are ultimately converted to both lactate and glucose. 2,5-Anhydro-D-mannitol (aHMol) mirrors symmetrically the $C_{1–3}$ moiety of β-2-deoxy-D-fructose, and as such has been employed as an analogue of the β-anomer of Fru.[17–18] AHMol is avidly phosphorylated in the liver,[19–20] and the extent of PME accumulation and of P_i trapping resemble that of Fru. AHMol is phosphorylated by hexokinase and by fructokinase.[21–22] Fructokinase has a higher affinity for the substrate, and in the presence of glucose plays a major role in the metabolism of aHMol. Thus, like Fru, aHMol metabolism is mainly restricted to the liver.[23]

AHMo11*P* is structurally identical to aHMo16*P*, an analogue of Fru6*P*, and is a substrate for 6-phosphofructokinase.[17–18] However, it is a poor substrate for the hepatic phosphofructokinase,[24] and only small quantities of aHMol(1,6)P_2 (3–10% of aHMo11*P*) accumulate even after prolonged incubation.[24–26] Because their ring structure is blocked, aHMo11*P* and aHMol(1,6)P_2 cannot be cleaved by phosphofructoaldolase. This precludes aHMol from being either a glycolytic substrate or a gluconeogenic precursor. Thus, the sugar is uniquely suited to study effects of 'Fru phosphorylation' on glycogenolysis, free of the confounding effects of the contribution of Fru itself to hepatic glucose and lactate output.

AHMol has been explored as a hypoglycaemic agent.[24–28] AHMol inhibits glycogenolysis.[25,27] *In vitro*, aHMo11*P*, but not aHMo1(1,6)P_2, is an inhibitor of glycogen phosphorylase. Inhibition of hepatic glycogen phosphorylase *a* by aHMo11*P* is competitive with $P_{i,}$[25,27] and the sugar behaves in this respect as Fru1*P*. In the present study, we employed aHMol as a dead-end Fru analogue, and evaluated its effect on glycogen phosphorylase *a*, maximally activated with *c*AMP. The experimental design involved verification of the nature of accumulating phosphate esters of aHMol, and attempts to elicit independent variations in aHMo11*P* and $P_{i,}$ by consecutive addition of the respiratory poison KCN and withdrawal of aHMol. We used ^{31}P-NMR to re-evaluate the relative role of accumulation of phosphate esters and of depletion of NMR-observable cytosolic P_i in the inhibition of glycogenolysis *in situ*.

MATERIALS AND METHODS

Materials

Reagents used for preparation of perfusate solutions were of regular *pro analysi* grade.

Preparation of anhydro-mannitol. AHMol was synthesized by reduction of the nitrous deamination product of 2-amino-2-deoxy-D-glucose.[29] The latter compound and sodium borohydride were purchased from Aldrich (Milwaukee, WI, USA).

Synthesis of aHMol1*P* and aHMol(1,6)P_2. For reference purposes, aHMol1*P* and aHMol-(1,6)P_2 were synthesized enzymatically by sequential phosphorylation of aHMol (65 mM) by hexokinase (from yeast, Boehringer Mannheim GmbH, Mannheim, Germany) and phosphofructokinase (from rabbit muscle, Sigma, St Louis, MO, USA) in the presence of a stoichiometric amount of Mg^{2+}·ATP, according to Bar-Tana and Cleland.[17]

Handling of animals and liver perfusion

Animals. Adult (about 250 g) well-fed male Wistar-derived *Pfd* rats were used in these experiments. Endoplasmic reticulum is a major depot of phospholipids, which give rise to a humpy-backed base-line distortion of ^{31}P-NMR liver spectra.[30] To curtail uncontrolled and unwanted induction of proliferation of the organelle by wood-impregnants in sawdust used for housing animals, we kept our rats on grids. The night prior to sacrifice, the animals had unrestricted access to sucrose to promote hepatic glycogen deposition. Rats were used in the morning, after anaesthesia with pentobarbital.

Liver perfusion. Isolation and perfusion of the liver have been described previously.[31] To minimize the contribution of P_i of the perfusion buffer to the total NMR P_i signal, we did not allow the perfusate leaving the liver to drain into the perfusion cell. Instead, we cannulated the draining *v. cava*, and continuously flushed the perfusion cell with non-recirculating isotonic NaCl.

The basic perfusion medium consisted of a balanced salt solution gassed with humidified O_2/CO_2 (19:1, at 37 °C and 1 atm). During the first equilibration phase of the experiment, the livers were perfused in recirculating mode under constant pressure (flow approx. 5 ml/g/min) with perfusate supplemented with 15 mM glucose, 2.7 mM lactate and 0.3 mM pyruvate. These conditions

suffice to suppress basal (not *c*AMP-stimulated) glycogen degradation.[32]

During the subsequent experimental phase the livers were perfused in single pass mode with nutrient-free buffer, at a constant flow rate of 50 ml/min (~3.3 ml/g/min). To study inhibition of phosphorylase *a*, we adopted a protocol in which hepatic glycogen phosphorylase is clamped in its fully activated *a*-form, by continuous exposure of the perfused liver to Bt_2cAMP (100 μM).[31] Other additions included aHMol (3.7 mM), and KCN (1 mM) as indicated.

Assays

Rate of glycogenolysis. The rate of glycogenolysis was calculated from the summed hepatic production of glucose, lactate and pyruvate in the perfusate (expressed as hexose equivalents/g liver/min).[31] Assuming that in the absence of added exogenous substrate, oxidative metabolism was mainly fuelled by glycogenolysis, we amended the glycogenolytic rate for oxidative glucose disposal. O_2 extraction was measured with a Clark electrode, and expressed as oxidized glucose equivalents.

Phosphorylase assay. For assessment of the degree of covalent activation of glycogen phosphorylase, we assayed phosphorylase activity in the glycogen-synthetic direction, using appropriate conditions for the measurement of phosphorylase *a* and of the total activity of phosphorylase (*a* and *b*).[33]

Extraction of livers for determination of aHMol1*P* and aHMol(1,6)P_2. Samples were taken after tightening a pre-positioned suture thread over the base of the isolated lobe. Consecutively (and in a clockwise manner) the smaller caudate semi-lunate Spigelian lobes, the right lobes, the median notched or cystic lobe, and finally the larger left lateral lobe were sampled. Thus, initially changes in total liver volume were minimized, and the perfusion was continued at constant flow rate. Tissue samples (0.1–0.5 g) were freezeclamped and extracted with 10 vol. of perchloric acid (0.9 M final), while adding the internal standard methylphosphonate (30 μmol/g tissue). After precipitation of proteins, the extracts were neutralized and desalted by addition of a stoichiometric amount of KOH/K_2CO_3 (13:2). Neutralized extracts were lyophilized and reconstituted in 3 ml Tris/acetate buffer (50 mM; pH 6.4), supplemented with 20 mM EDTA to complex paramagnetic cations, thus improving resolution of ^{31}P-NMR spectra of the extracts.

^{31}P-NMR spectroscopy

Acquisition and analysis of high resolution spectra of liver extracts for determination of aHMol1*P* and aHMol(1,6)P_2. Relaxed ^{31}P-NMR spectra were acquired on a Bruker AMX 360 spectrometer. We accumulated blocks of 1024 scans using a 90° pulse with a repetition time of 20 s. Spectra were analysed in the frequency domain, after Fourier transformation. Quantitation was based on comparison of the integrated peak area under the methylphosphonate standard, and the combined aHMol1*P* and aHMol(1,6)P_2 signals. At pH 6.4 the latter signals segregate (0.16 ppm apart). Their identity was confirmed by internal addition of the reference compounds. Because of their marginal resolution at the base line level, their relative intensities were analysed by fitting two Lorentzians, using a commercial simulation package (WIN-NMR, Bruker, Karlsruhe, Germany).

Acquisition of spectra on perfused liver. ^{31}P-NMR spectra were obtained in a Bruker 4.7 T horizontal magnet with a 30 cm bore. We accumulated blocks of 2048 scans using 30° radiofrequency pulses with a repetition time of 45 ms. Each scan consisted of 256 data points, collected with a dwell time of 98.1 μs (63 ppm sweep-width).

The choice of pulse parameters was inspired by the following considerations:

(i) spectra were analysed (see below) by an algorithm operating in the time domain whereby only the initial part of the FID signal that remains discernible from the noise contains useful information. We used a repetition time of 45 ms, about four times the effective signal damping time constant, T_2* (shim $w_{1/2}$: ~0.4 ppm at 81 MHz). Transverse magnetization coherence build-up was suppressed[34] by cycling of the phase of the radiofrequency pulse. This was effective, since no regrowth of the FID signal towards the end of the pulse interval g and no phase or amplitude anomalies across the Fourier transformed spectrum were observed.

(ii) Differences in spin-lattice relaxation behaviour (T_1) of intra- and extracellular P_i can be exploited to selectively saturate the long-lived spin system. This effectively suppresses signal contribution from the extracellular compartment,[5] which is characterized by a *ca*. 10-fold longer T_1.[5,31] With the repetition time (45 ms) dictated by the previous consideration, we selected a pulse angle (30°) to optimize the contrast between intra- and extracellular P_i.

Constancy of pulse duration and amplitude, over all experiments, was verified on an oscilloscope, through a directional coupler. To ensure reproducibility of delivered power, tuning and matching of the resonator to the transmitter–receiver chain was optimized for each experiment. Variation of the electrical load of the coil was negligible, and independent of the liver volume, since livers were immersed in isotonic saline, filling the

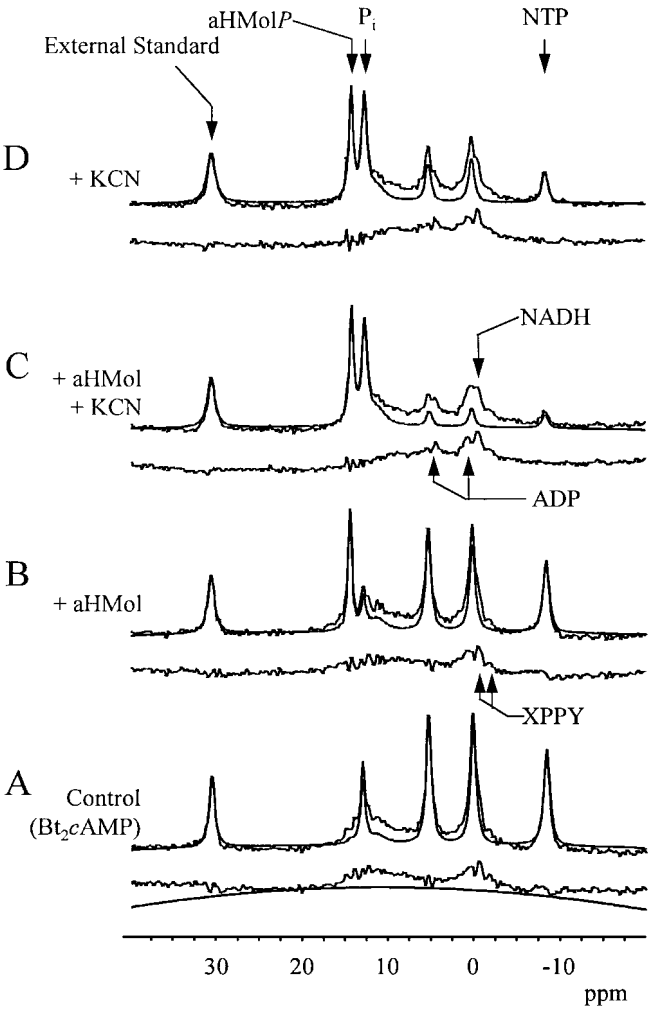

Figure 1. ^{31}P spectra of perfused liver. We show representative spectra, corresponding to the four consecutive experimental phases shown in Fig. 2(A). Each spectrum results from the addition of five contiguous acquisition blocks (1.5 min/block) acquired at the end of each experimental phase. An averaged PME signal corresponding to the basal PME signal has already been subtracted (see Methods). From bottom to top: (A) control spectrum of the liver after 15 min exposure to 100 μM Bt_2cAMP; (B) 30 min after the subsequent addition of 3.7 mM aHMol; (C) 15 min after subsequent addition of 1 mM KCN.; (D) 15 min after withdrawal of aHMol in the sustained presence of KCN. We show: (a) the Fourier-transformed time domain signals (solid line); (b) the sum of fitted components (smooth line through (a)); (c) the non-fitted residue (stacked below the spectrum). Prior to Fourier transformation, the time domain signal was zero-filled up to 2^{10} data points. Spectra (a) and (c) are treated with the base line correction function (second degree polynomial) shown in the bottom panel. Peaks used for the construction of Fig. 2(A) (P_i; aHMol*P* or ΔPME; and the *β*-phosphate of NTP) are identified in the top panel. Tentative assignments are given for metabolites as they appear in the residue (XPPY: nucleotidyl pyrophosphate, e.g. UDPGlc)

measurement chamber to a constant volume.[31] The latter was centered within the volume of an open-gap foil-resonator, which ensured a homogeneous radiofrequency excitation field over the whole liver.[35]

Processing and analysis of spectra of perfused liver. Accurate determination of signal intensities in the *ortho*-phosphate region is particularly cumbersome. An extremely broadened PDE signal, arising from anisotropically moving membrane-bound phospholipids,[30] underlies a multitude of narrow but unresolved (overlapping) signals arising from metabolites, which are recorded with a low signal-to-noise ratio at the short time-resolution sought in this study (1 spectrum/1.5 min).

Spectra (Fig. 1) were analysed in the time domain, using the MRUI package.[36] The signal was fitted to a sum of exponentially damped sinusoids, by an iterative nonlinear least squares algorithm, based on the VARiable PROjection (VARPRO) method.[37] Convergence behaviour of the iterative algorithm was improved by avoiding over-parameterization of the model function to be fitted. This was achieved by replacing variables by constants, whenever they are known *a priori* from high quality data, and by linking variables that are known to co-evolve in a predictable manner.

Boundary conditions. (i) A common zero-order phase was imposed on all peaks. The first-order phase term was estimated from the calculated delay time, between pulsed excitation and the first sampled time point that was used (see below). (ii) We fitted 11–12 signal poles: the external standard, a PME and PDE (if resolved) cluster, the increment in PME, free P_i, and the *γ*-, *β*- and *α*-phosphate signals of NTP. The latter were forced to obey the following constraints: the *α*- and *γ*-phosphate doublets of NTP (1:1 intensity ratio) and the *β*-phosphate triplet (1:2:1 intensity ratio) were effectively fitted as multiplets, reflecting their homonuclear splitting (J_{PP}: 16 Hz).[38] The singlets composing each multiplet share a common damping factor. Initial resonance frequencies were selected by manual peak-picking (using the Fourier-transformed spectral representation of the experimental signal).

Subtraction of background signal. We wanted to illustrate changes in aHMol*P* (PME) and P_i signals, brought about by the administration of aHMol and KCN. Unresolved PME and PDE signals present in the control spectra and persisting throughout the experiment were not of interest. (i) Omission of the two to three initial data points in the time-domain amounts to a filter on the broad hump, originating from membrane-linked PDE. The residual membrane-linked PDE signal was fitted as a single Lorentzian peak with $w_{1/2}$ of ∼200 Hz. Cytosolic PDE signals were occasionally fitted as narrow resolved metabolites. All this had minor effects on the signal intensities of neighbouring P_i and PME signals. (ii) We analysed the summed spectra of the control phase of the individual experiments, to determine the 'average' peak shape of background PME signal. The PME (and PDE) signal demonstrate inhomogeneous peak broadening, due to the chemical-shift variability of compounding signals

(ca. 1 ppm range). However, the quality of the data usually only allowed for a 'mathematical' fit to a single exponentially decaying PME signal pole. A reconstructed time-domain signal ($w_{1/2}$: 1.2–1.4 ppm), corresponding to the 'average' PME found in basal conditions, was subtracted from the experimental signals in which the PME and P_i signals showed the changes induced by the administration of aHMol, and of KCN. The resulting 'difference' spectra were analysed for changes in the PME and P_i signals.

Imposing peak shape and peak position. The administration of aHMol induced reciprocal changes in P_i and PME. As analysis of the one signal became more precise, estimates for the other became less certain. Both signals stem from the same cytosolic compartment, and thus experience identical peak broadening and sense the same pH. (i) Both the residual P_i and increment in PME (aHMol*P*) were forced to abide by a common peak shape ($w_{1/2}$: 0.5–0.7 ppm), determined by fitting the summed spectra of the end stages of the aHMol, and KCN phases (Fig. 1). (ii) Inaccuracies in the P_i signal, weakened as it was drained toward accumulating PME, were recognized from scatter on the estimated resonance frequency and/or the derived pH value. For such samples the peak position of the weaker signal was dictated by the pH derived from the stronger signal (see below for titration constants). (iii) Also for the NTP singlets, an average (derived from the summed control spectra) peak width was imposed.

Sliding rule. Individual blocks (1.5 min/spectrum) were analysed during the transition phases. To improve the signal-to-noise ratio, a sliding rule was applied for analysis of the spectra, when the time resolution was no longer critical (slow steady rate of changes in the various metabolites). Spectra were summed by 3–5. An uneven number of blocks was taken to facilitate attribution of the derived value to the central time point.

Inspection of results. Imposing signal damping time constants upon the PME, P_i and NTP signals, and using a sliding rule is in the limit equivalent to a two-dimensional fit, whereby information obtained in successive spectra is used to its fullest extent under the tacit assumption that peak widths and positions are invariant. Imposing peak widths (removing nonlinear terms from the algorithm to be solved) dramatically speeds up fits, and reduces the number of failures to reach convergence. Conversely, faulty assignment of peak widths has profound effects on derived signal intensities.

To evaluate whether the adopted strategy was effective and acceptable, we compared results, before and after imposing peak widths and positions. On average, fitted parameters evolved in time in a superimposable fashion, irrespective of whether signal damping time constants were left free or were forced in the individual spectra. In the latter case, the evolution of the fitted signal intensities was smoothened, attesting to the beneficial filtering effect of this strategy.[19]

Both the P_i and aHMol*P* signals experience time averaged chemical shift inhomogeneities due to ongoing metabolism and tissue acidification. These effects will be most pronounced at the onset of aHMol and KCN administration (see discussion of results, below). The two phosphate groups in aHMol(1,6)P_2 are stereochemically identical, and hence co-resonate.[39] The signal arising from aHMol1*P* cannot be resolved from that of aHMol(1,6)P_2 under *in vivo* conditions. From our knowledge of high resolution spectra of extracts, the simultaneous presence of comparable amounts of both species could result in some peak broadening (< 0.05 ppm at pH 7.2). AHMol and KCN each induced a pH drop of less than 0.3 pH units (drop in pH with respect to value, prior to the manipulation, maximum of 4 experiments), spread over ~3–6 consecutive scans. This translates into a shift never larger than 0.06–0.13 ppm/scan for aHMol1*P* and P_i, respectively, in the affected regions (prior to establishment of the new steady state). Not allowing the peak shape to vary accordingly (less than 20% of the imposed width) introduces a corresponding error in the estimated peak intensity. When inspection of the residue revealed that linking the peak width of P_i and PME introduced systematic errors (base line wiggles secondary to erroneous peak shape assignements) then this constraint was relaxed. In all cases, peak widths of P_i and PME were larger than the peak width of the water shim signal, but smaller than widths found for the NTP singlets.

Peak widths of NTP singlets and of P_i and PME were imposed. They were mainly determined by the 'Lorentzian' behaviour of well-resolved intense signals. Because the peak widths of the α- and γ-phosphate signals of NTP and the aHMol*P* signals were linked to the width of other signals (β-phosphate of NTP and P_i, respectively), they are minimally contaminated with signal originating from other nucleotidyl pyrophosphates (UDPGlc, ADP, etc.) or from neighbouring monophosphate esters, respectively. The latter weaker chemical species can be recognized in the residue (Fig. 1) after deconvolution of the intense NTP and aHMol*P* signals. Unfortunately, AMP cannot be resolved from aHMol*P*.

pH titration curves. We titrated a mixture of Mg^{2+}·ATP, P_i, and aHMol1*P* (~5 mM each) in isotonic KCl, with small aliquots of 1 M HCl and NaOH (pH range 3–9). Partially saturated spectra (pulse: 45°; *TR*: 1 s; scans: 64) were acquired at 8.5 T at 37 °C. The resulting titration curves were fitted by standard methods to the regular NMR representation of the Henderson–Hasselbalch equation. Estimates for the pK_a, and the chemical offset values δ_{HA}, δ_{A^-} (in ppm from the resonance for the α-phosphate of Mg^{2+}·ATP), for the protonated and dissociated forms, respectively, were 6.74, 10.64,

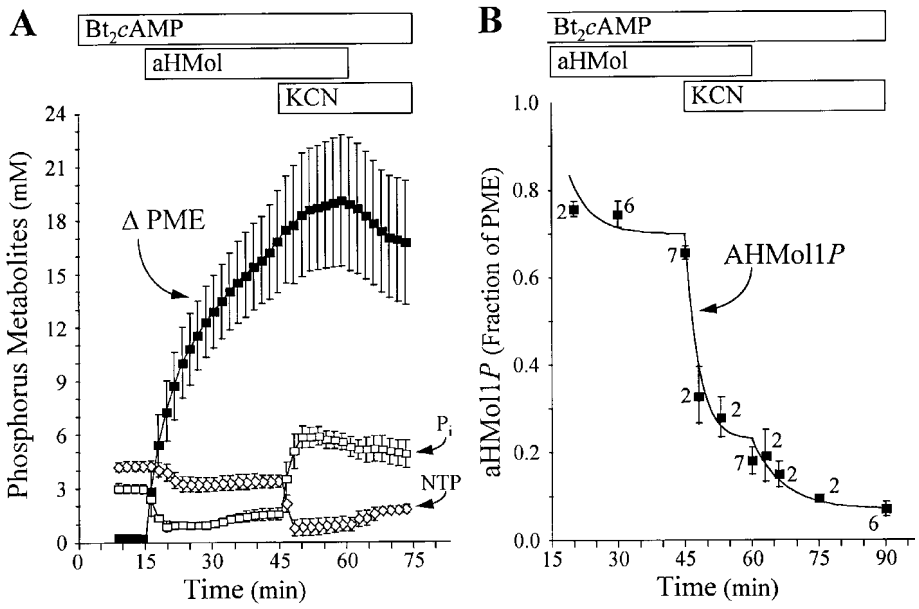

Figure 2. Phosphorylation of 2,5-anhydro-D-mannitol. Livers ($n = 4$) were continuously exposed to Bt_2cAMP (100 μM). The time of exposure to aHMol (3.7 mM) and KCN (1 mM) is indicated by the labelled bars. Panel A: evolution of P_i (□), the increment in PME (■), and the evolution of NTP (◇), as evaluated by *in situ* ^{31}P-NMR. Panel B: ratio of aHMol1*P* (■) as a fraction of total aHMol-linked phosphorus (equivalent to the increment in PME in panel A). Liver lobes (five to six per liver) were sampled from seven livers at the consecutive time points indicated. Sampling overlapped, but samples were not taken at all time points in each liver. Averages ± SEM are shown. A smooth exponential decay curve was fitted through each of the experimental phases. This curve is the function $\alpha(t)$ of eqn 1, and is used in the fits shown in Fig. 4. The discontinuities in the curve accomodate the fit of discontinuities in the glucose output curves (Fig. 4, top panels), and were justified by the inspection of time courses in individual livers (not shown here)

13.25, and 6.29, 11.02, 14.52 for P_i and aHMol1*P*, respectively.

Quantitative analysis of ^{31}P-NMR spectra. Peak intensities were calibrated against an external hexachlorocyclotriphosphazene standard (equivalent to 37.5 μmol of ^{31}P), relaxed by the addition of a Cr(III) complex.[40] Signals were weighted for saturation effects. For calculation of saturation factors,[41] we adopted T_1 values (at 4.7 T) from literature:[42] PME, 1.30 s; P_i, 0.64 s; the β-*P* of NTP, 0.18 s. These are within the error range of our own estimates.[31]* The T_1 value for the external standard was 0.21 ± 0.08 s. Such measurements are lengthy, and are limited by the metabolic stability of the preparation under study. The analysis suffers from poor signal/noise ratios, which become particularly cumbersome when the data are best fit by a two-compartment model (i.e. P_i distributed over the intra- and extracellular compartments). Our estimate on the between-liver reproducibility (variation coefficient) for each of these T_1 estimates ($n = 2$) ranges from 12% for the NTP signals to 35% for the P_i and PME signals. We assumed that T_1 values for the PME signal of spectra, acquired in control liver, apply to Fru1*P* and aHMol1*P* and aHMol(1,6)P_2. No methods are available to correct for likely changes in T_1, secondary to changes in pH and the apparent affinity constant of titrated phosphate functions for complexation of relaxing polyvalent cations.

The liver volume was estimated by weight. Intracellular concentrations are expressed in mM, assuming that the intracellular water space comprised 70% of the wet weight of excised liver.[15]

Statistics and analysis of kinetics

Data are reported as means ± SEM. Rates of glycogenolysis were correlated with changes in P_i and PME levels. NMR and metabolic data were sampled with a different time base. Estimates for the glycogenolytic rate coincident with NMR data points were calculated by linear interpolation. The rate of glycogenolysis (ν) was then

*In the original report by [31], an erroneous value was reported for PME.

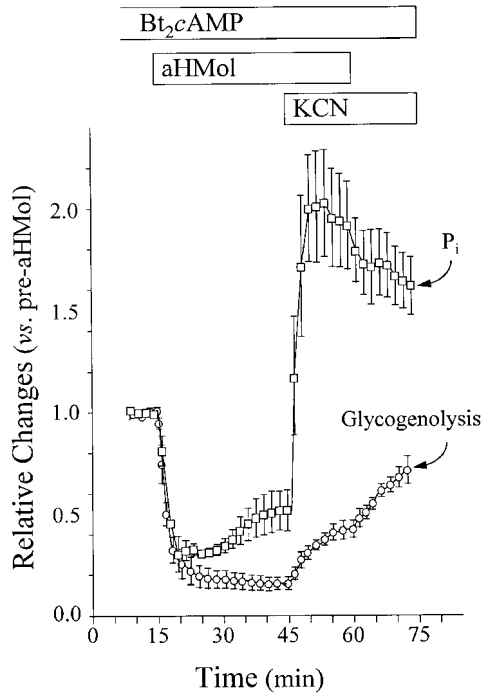

Figure 3. Comparison of the effects of 2,5-anhydro-D-mannitol and KCN on the concentration of cytosolic P_i and the rate of glycogenolysis. Livers [same experiments as in Fig. 2(A)] were continuously exposed to Bt_2cAMP (100 μM). The time of exposure to aHMol (3.7 mM) and KCN (1 mM) is indicated by the labelled bars. The rate of glycogenolysis (○), and the level of hepatic P_i (□) are shown as means ± SEM ($n = 4$). The data are scaled relative to the average rates and levels observed in each individual liver during the last 5 min of the control phase of the experiment (after full activation of glycogenolysis by exposure to Bt_2cAMP)

fitted to a Michaelis–Menten-type equation, accommodating for the degree of saturation by P_i and for linear competitive inhibition by aHMol1*P*.

A model equation accommodating the regular form of the Michaelis–Menten equation failed to converge. As the system remained far from saturation by P_i under all conditions (the situation only worsened in the presence of inhibitor), V_{max} (maximal catalytic rate) could not be estimated reliably. We therefore reduced the equation to the limiting case for $[P_i]$ approaching 0 [eqn 1]. This equation is approximated by Michaelis–Menten kinetics when the substrate concentration is much smaller than K_m.[43]

This reduces the Michaelis–Menten constants, V_{max} and K_m, to a new 'linear' constant V_{max}/K_m.

$$\nu = (V_{max}/K_m)[P_i]1/(1 + [\mathcal{F}\{\alpha(t)\} \cdot \Delta[\mathrm{PME}]]/K_I) \quad (1)$$

with $\Delta[\mathrm{PME}]$ being $[\mathrm{PME}] - [\mathrm{PME}]_0$, the change in PME level, with respect to $[\mathrm{PME}]_0$, prior to aHMol administration and with $\mathcal{F}\{\alpha(t)\}$ (see implementations in the consecutive panels of Fig. 4) being the fraction of $\Delta[\mathrm{PME}]$ considered to be inhibitory; $\alpha(t)$ is [aHMan1*P*]/$\Delta[\mathrm{PME}]$ as a function of time, from Fig. 2(B), and K_I is an inhibition constant.

The equation, which remains nonlinear in K_I, was fitted by standard nonlinear orthogonal (three-dimensional: ν, $[P_i]$, $\mathcal{F}\alpha(t)\cdot\Delta[\mathrm{PME}]$) regression techniques.[44] Results of the fit are reported with the standard error on the estimated constants.

RESULTS

Effectiveness of the phosphorylase *a*-clamp

We clamped glycogen phosphorylase in its active *a*-form by continuous exposure of the perfused livers to 100 μM Bt_2cAMP. This results in maximal activation of glycogenolysis within 10 min.[31]

Phosphorylase *a* levels are not invariant after Fru administration.[1,45] Activation of the enzyme with Bt_2cAMP, prior to testing the effects of aHMol, allowed us to evaluate changes in glycogenolysis exclusively due to changes in the kinetic behaviour of phosphorylase *a*, without unwanted interference from conversion between the inactive *b*-and active *a*-form of the enzyme. The exclusive study of the *a*-form is physiologically relevant, since in liver, contrary to muscle, glycogenolysis is solely catalysed by phosphorylase *a*. Indeed, hepatic glycogenolysis remains insignificant under all conditions in the *gsd/gsd* rat, which cannot activate phosphorylase.[46] An additional advantage of the co-administration of Bt_2cAMP is that it is likely to suppress formation of aHMol(1,6)P_2, arising from phosphofructokinase activity, which is suppressed by *c*AMP.

The effectiveness of the Bt_2cAMP-treatment was inferred from the fact that hepatic glucose production rose within 10 min to a high and stable rate (5.5 ± 0.9 μmol/g/min; $n = 4$), compatible with full activation of the enzyme.[31] No tissue samples could be procured during the NMR experiment, but we could confirm on liver lobes sampled at the end of the experiment that phosphorylase was essentially present in the active *a*-form ($95 \pm 3\%$ of the total enzyme), and that residual glycogen levels (≥180 μmol glucose equivalents/g) sufficed to maintain a glycogenolytic response.

Phosphorylation of aHMol in perfused liver

After exposure to 3.7 mM aHMol, substantial amounts of aHMol*P* accumulated in the liver, essentially at the expense of P_i, with little decrease in NTP [Fig. 2(A)]. Most of the accumulated phospho-ester was present as aHMol1*P* [Fig. 2(B)], confirming reports in the litera-

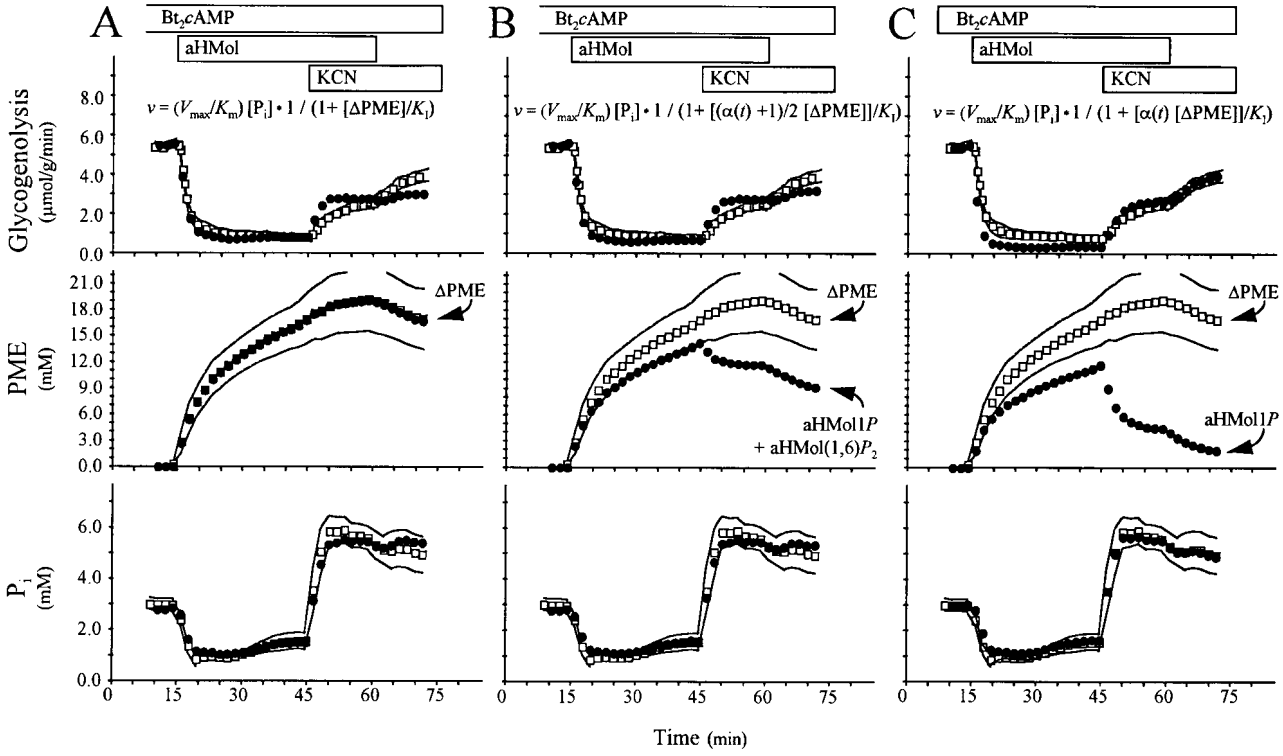

Figure 4. Inhibition of glycogenolysis and depletion of cytosolic P_i by 2,5-anhydro-D-mannitol. Livers [from Fig. 2(A)] were continuously exposed to Bt_2cAMP (100 μM). The time of exposure to aHMol (3.7 mM) and KCN (1 mM) is indicated by the labelled bars. Averages (absolute values; □) ±SEM envelope ($n = 4$) are shown. The data (□) are fitted (●) to the kinetic equation [Eqn 1], shown in the top panel. 'Corrected' values shown (●) correspond to the orthogonal projection of the raw data (□) on the fitted surface (ν, [P_i], [relevant PME fraction]), given by the equations in the top panels. Panel A: the increment in the PME levels (ΔPME) is treated as if it were entirely composed of a single monophosphorylated inhibitor (aHMol1*P*). Panel B: both the aHMol1*P* and aHMol(1,6)P_2 are treated as equivalent inhibitors. ΔPME is corrected for 2:1 phosphorus stoichiometry in accumulating aHMol(1,6)P_2. Panel C: only aHMol1*P* enters the equation as an inhibitor. Corrections of ΔPME in Panels B and C rely on the function $\alpha(t)$, as known from Fig. 2

ture.[24–26] A partial recovery of P_i after the initial dip was observed.

For the study of the relative effectiveness of aHMol1*P* accumulation and of P_i depletion as mechanisms contributing to inhibition of hormone-stimulated glycogenolysis, we intended to elicit independent changes in these two parameters by the subsequent addition of the respiratory poison KCN. This resulted in a sharp decrease in NTP levels, and a complemetary rise in P_i [Fig. 2(A)]. Although AHMol1*P* is a poor substrate for the hepatic phosphofructokinase,[24] the chemical hypoxia caused by KCN sufficed to induce the enzyme into conversion of aHMol1*P* into aHMol(1,6)P_2 [Fig. 2(B)]. The loss of NTP and the possible rise in AMP, induced by KCN, may have sufficed to stimulate phosphofructokinase.[47] AMP was barely detectable in extracts from liver prior to KCN administration, presumably because the drop in P_i, secondary to aHMol administration, may have suppressed accumulation of AMP due to de-inhibition of AMP deaminase.[2] After KCN administration, we estimated from ^{31}P-NMR on the extracts of the livers (shown in Fig. 2B) that AMP plus IMP could have risen up to 1.7 mM.

Metabolic instability of aHMol*P* precludes lengthy experimental assessment of its exact T_1 relaxation time, and hence of correct saturation factors. Over the period where both aHMol and KCN were present, the average PME level estimated from *in situ* NMR experiments [18.5 ± 3.7 mM, Fig. 2(A)] was slightly higher than the sum of all aHMol*P* (16.8 ± 1.2 mM, $n = 11$) found in relaxed spectra of extracts of liver lobes [Fig. 2(B)] harvested at that time. Both values are expressed relative to the estimated cell volume (70% of tissue mass). This reflects on the applicability of the estimated T_1 relaxation time.

Subsequent withdrawal of aHMol facilitated a further loss of remaining aHMol1*P*, mostly by conversion to a HMol(1,6)P_2 in the absence of *de novo* aHMol1*P* formation. Hydrolysis of aHMol phospho-esters may be responsible for the decline in the PME signal. AHMol(1,6)P_2, a competitive inhibitor of fructose-1,6-bisphosphatase,[24] is lost upon prolonged incubation,[48]

possibly by dephosphorylation. Withdrawal of aHMol also resulted in a partial recovery of NTP levels, presumably secondary to decreased use for aHMol phosphorylation and to improved glycolytic NTP generation. Phosphorus originating from the PME compartment appears to be used for expansion of the NTP pool. The decline in aHMol1*P* in favour of aHMol(1,6)P_2, allowed us to evaluate the inhibitory effectiveness of both (see below).

Qualitative analysis of the effects of 2,5-anhydro-D-mannitol and KCN on maximal glycogenolysis

Reference values for hepatic P_i and for glycogenolysis in the Bt_2cAMP-treated livers were recorded prior to the administration of aHMol. Subsequent perfusion of the livers with aHMol resulted in a drop in P_i, attributable to aHMol*P* accumulation (Fig. 3). Initially, glycogenolysis and P_i evolved in parallel. However, after about 5 min their evolution progressively diverged. P_i partially recovered, but glycogenolysis remained inhibited. Excessive inhibition of glycogenolysis (to $14 \pm 3\%$ of control) over the drop in P_i (to not lower than $31 \pm 2\%$ of control; Fig. 3) may be explained by the inhibitory effect of aHMol1*P*, which meanwhile continued to accumulate (Fig. 2). Presumably, phosphate needed for the continued accumulation of aHMol1*P* is extracted from the extracellular perfusate.

Changes after the addition of KCN further illustrate the role of P_i and of aHMol1*P* as determinants of phosphorylase *a* activity. Addition of the respiratory poison KCN (1 mM) resulted in a rapid increase of P_i, at the expense of NTP [Fig. 2(A)] and in a partial conversion of aHMol1*P* into aHMol(1,6)P_2 [Fig. 2(B)]. However, the stimulation of glycogenolysis by KCN is much smaller than the increase in P_i; for instance 5 min after the addition of KCN, the cytosolic P_i level had risen to a value exceeding control levels 2 ± 0.25-fold, but the rate of glycogenolysis was only $32 \pm 3\%$ of that in the control phase [Fig. 3(A)]. This attests to residual inhibition by phosphorylated aHMol products. The rate of glycogenolysis progressively increased [to $45 \pm 4\%$ of rates in the control phase; Fig. 3(A)], presumably secondary to a slow loss of aHMol1*P* in favour of aHMol(1,6)P_2.

After subsequent withdrawal of aHMol, the glycogenolytic activity rose further, although inorganic P_i tended to drop (Fig. 3). The stimulation of glycogenolysis can then only be explained by the loss in PME [Fig. 2(A)] and further conversion of aHMol1*P* into the bisphosphate [Fig. 2(B)]. In the quantitative analysis that follows (next section) we will see that only the evolution of aHMol1*P* levels covers the dynamic range needed to explain the observed stimulation of glycogenolysis.

Quantitative analysis of the effects of 2,5-anhydro-D-mannitol and KCN

We put the above conclusions to the test by fitting the data to the proper kinetic equations. By applying proper scalar corrections (see methods) we could also replace relative changes (Fig. 3) with absolute values (Fig. 4), to get some idea of the nominal values of the applicable kinetic constants.

The data can be fitted to a kinetic model accommodating P_i dependence and competitive inhibition by aHMol phosphorylation products. Three experimental phases can be discerned: (i) the substrate P_i drops and the inhibitor aHMol1*P* appears; (ii) KCN induces an increase in P_i—However, concomitantly a substantial fraction of the inhibitor aHMol1*P* is converted into aHMol(1,6)P_2; (iii) after withdrawal of aHMol (in the presence of continued exposure to KCN), the remainder of aHMol1*P* is converted into aHMol(1,6)P_2. The experimental phases thus describe a curved trajectory on the (v, [P_i], [inhibitor] (surface, to which eqn 1 can be fitted. As the system was never saturated with its substrate P_i,[31] we fitted the data to a reduced equation, linear in the substrate concentration (see the section Statistics and analysis of kinetics).

We wanted to predict the observed glycogenolytic activity (v, dependent variable) from observed levels of P_i and changes in PME ([P_i], Δ[PME]; independent variables). We chose an orthogonal regression technique,[44] in which all variables are treated as statistically equivalent variables (each absorbing error). The summed squared orthogonal projection of the data (v, [P_i], Δ[PME]) to the fitted surface [eqn 1] is minimized. The error (difference between observed values (□) and their 'corrected′ orthogonal projections (●) in Fig. 4) is then a direct reflection of the sensitivity (or partial first derivative of the error function) of the result to variation of that parameter. We analyzed three scenarios:

(i) accumulating PME is composed of a single inhibitory species, aHMol1*P* [Fig. 4(A)]. The fit shows that this appears to be a fair approximation prior to the addition of KCN. However, after addition of KCN, the fit shows a tell-tale systematic error distribution. Then, corrected (fitted) P_i apparently first is systematically underestimated, then overestimated. The corrected rate of glycogenolysis shows sign-wise the opposite error distribution. The fact that PME is treated as essentially error-free reflects the nature of competitive inhibition: large changes in inhibitor/K_I are needed for the system to respond in an asymptotic manner. Hence, in this fit procedure most of the error is absorbed by the (v, [P_i]) pair, which shows identical (but sign-wise opposite) sensitivity. This is a direct consequence of the fact that we are working in the non-saturated linear part of the

Michaelis–Menten curve, where v is maximally responsive to changes in $[P_i]$.

(ii) Correcting the PME curve for the stoichiometric bias introduced by the conversion of aHMol1*P* into aHMol(1,6)P_2, only marginally improved the result [Fig. 4(B)].

(iii) Allowing only aHMol1*P* to act as an inhibitor substantially improved the fit [Fig. 4(C)]. Apparently, aHMol1*P* is the inhibitory species, and the bis-phosphorylated compound is at best a poor inhibitor.

AMP generated by the consumption of ATP is unlikely to affect our results significantly. From the inspection of the extracts [used in Fig. 2(A)], we can conclude that the combined levels of AMP and IMP were never larger than 1.7 mM (values found after KCN administration). While AMP (and IMP) stimulates phosphorylase *a in vitro*, the effect on hepatic phosphorylase *a* is small, and the enzyme should already be substantially saturated with AMP in the well oxygenated liver.[49]

We calculated hepatic glycogenolysis from the summed hepatic glucose, lactate and pyruvate output, amended for oxidative glucose disposal as estimated from O_2 extraction data. The basal rate of O_2 extraction (2.1 ± 0.3 μmol O_2/g liver/min) amounts to ~7% of the reported glycogenolytic rate before aHMol administration. In absolute amounts O_2 extraction drops (to 1.5 ± 0.1 μ O_2/g liver/min) after aHMol administration, presumably reflecting reduced substrate availability and possibly P_i dependence of oxidative phosphorylation. On average, the contribution of O_2 extraction amounts to ~67% of the reported glycogenolytic output after aHMol administration. Its fractional importance stems from the deep dip in glucose output. The fit results [Fig. 4(C)] suggest that, under conditions of reduced glucose availability, a substantial fraction of O_2 extraction has to be attributed to oxidation of endogenous substrates other than glycogen (fatty acids and amino acids). After addition of the respiratory inhibitor, KCN, oxidative outflow of glycogenolytic products (and of non-glycogen substrate) becomes negligible.

Because the enzyme is far from saturated by its substrate, no *in situ* estimate for the K_m for P_i can be produced. In the presence of lyotropic salts, mimicking the cytosolic milieu, this K_m may be as high as 30 mM.[49] *Pseudo*-linear dependence on P_i levels (V_{max}/K_m: 1.8 ± 0.24/min) confirms that the K_m value of the enzyme for P_i exceeds by far the actual cytosolic P_i levels. Our estimate for the K_I for aHMol1*P* (1.6 ± 0.35 mM) compares well with *in vitro* determined values for K_I values for aHMol1*P* (0.7–2.4)[25,27] and for Fru1*P* (1.2–4),[13–14] although these values may not always have been obtained under physiologically relevant incubation conditions (see effect of lyotropic salts[49]).

DISCUSSION

Mechanism of inhibition of glycogen phosphorylase *a* by fructose

The kinetic behaviour of phosphorylase *in situ* is dictated by the fact that the enzyme is far from saturated by its substrate, P_i.[31] This produces opportunities for regulatory control: (*i*) metabolically induced changes in P_i exert control over the catalytic activity of phosphorylase *a*;[31] (*ii*) the catalytic rate is under these circumstances inversely proportional to the apparent K_m value (see K_m in the denominator of V_{max}/K_m), or in other words, the system becomes sensitive to competitive inhibitors.

Inhibition of glycogenolysis by aHMol1*P* reflects both trapping of P_i, and a rise [times $(1 + [\text{aHMol1}P]/K_I)$] of the apparent K_m value of the enzyme for P_i secondary to effective competition by aHMol1*P*. Both effects of aHMol are interrelated, as P_i trapping is a consequence of early aHMol*P* accumulation. The relative contribution of either factor can be appreciated from eqn 1. At any given level of aHMol1*P*, the glycogenolytic rate depends linearly on P_i [derivative with respect to $[P_i]$: (V_{max}/K_m). $1/(1+[\text{aHMol1}P]/K_I)$]. The effect of P_i trapping is accentuated by concomitant aHMol1*P* accumulation. Inhibition by aHMol1*P* is an asymptotic function [first derivative with respect to [aHMol1*P*]: $-(V_{max}/K_m)\cdot[P_i]\cdot(1/K_I)\cdot(1 + [\text{aHMol1}P]/K_I)^{-2}$]. Competitive inhibition by aHMol1*P* is observed, since two necessary conditions are fulfilled: (*i*) competitive inhibition cannot be overcome by substrate saturation, since the enzyme is far from saturated (see above); and (*ii*) affinity for aHMol1*P* is sufficiently high (or K_I sufficiently low) for the system to become appreciably sensitive to accumulation of this inhibitor in the biological range. In conclusion, our data confirm that, under conditions prevailing in the intact liver, Fru1*P*, or at least its analogue aHMol1*P*, is indeed a competitive inhibitor of phosphorylase *a*. Inhibition becomes observable precisely because the enzyme is not saturated with P_i.

On the regulation of hepatic glycogen turnover

Rates of glycogenolysis and of glycogen repletion are governed by glycogen phosphorylase and synthase, respectively.[50] Both enzymes are interconverted between active and inactive forms by phosphorylation–dephosphorylation cycles, which operate in a fashion so as to disfavour simultaneous activation of both enzymes,[51] and thus are geared to minimize cycling of phosphorylated glucose residues through a futile glycogen cycle. The *in vivo* maximal glycogenolytic activity[31] exceeds maximal glycogen deposition rates ca. 5-fold. Residual activity of incompletely inactivated glycogen phosphorylase can thus give rise to measurable futile cycling of glycogen.[52–53] For effective glycogen deposition ever to occur,

besides covalent inactivation of the enzyme, additional non-covalent regulation restraining phosphorylase activity *in situ* may be essential.

Plugging in a K_m value for P_i of 30 mM[49] in our estimate for V_{max}/K_m (1.8/min) translates to a V_{max} of about 50 μmol/g/min, similar to values found *in vitro* and far in excess of maximal *in vivo* rates of glycogen breakdown. Our estimate for free cytosolic P_i confirms published data.[15–16] At a K_m for P_i of 30 mM and a cytosolic level of 3 mM, only ca. 10% of that maximal catalytic potential is expressed. In summary, our results confirm that the *in situ* activity of phosphorylase *a* is but a fraction of its full catalytic capacity, and P_i availability and the presence of inhibitors (PME) may be decisive factors in the control of that catalytic potential.

Fru promotes hepatic glycogen deposition, despite paradoxical covalent activation of phosphorylase.[54] Suppression of futile glycogen cycling by high doses of Fru[55–56] may contribute to the glycogenic effect of Fru. Here, we have presented a quantitative evaluation of the inhibition *in situ* of phosphorylase *a*-catalyzed glycogenolysis by P_i depletion and accumulation of the Fru1*P* analogue, aHMol1*P*. The combined effects suffice to suppress the catalytic activity of phosphorylase *a*.

Acknowledgements

This work was supported by grants 3.0064.94 from the Fund for Medical Scientific Research (Belgium), G.0360.98 from the Fund for Scientific Research–Flanders (Belgium) and OT/93/31 from the Research Council of the Katholieke Universiteit Leuven.

REFERENCES

1. Van den Berghe, G. Biochemical aspects of hereditary fructose intolerance. In Normal and Pathological Development of Energy Metabolism. (Hommes, F. A. and Van den Berg, C. J., *Eds.*) pp. 211–228. Academic Press, London (1975).
2. Van den Berghe, G. Fructose: metabolism and short-term effects on carbohydrate and purine metabolic pathways. *Prog. Biochem. Pharmac.* **21**, 1–32 (1986).
3. Gitzelmann, R., Steinmann, B. and Van den Berghe, G. Disorders of fructose metabolism. In The metabolic Basis of Inherited Disease. (Scriver, C. R., Beaudet, A. L., Sly, W. S. and Vallé, D., *Eds.*) Ed. 6, Vol. **1**. Chp. 11, pp. 399–424. McGraw-Hill Information Services, Maidenhead (1989).
4. Mayes, P. A. Intermediary metabolism of fructose. *Am. J. Clin. Nutr.* **58**, 754S–765S (1993).
5. Iles, R. A., Griffiths, J. R., Stevens, A. N., Gadian, D. G. and Porteous, R. Effects of fructose on the energy metabolism and acid-base status of the perfused starved rat-liver. A ^{31}phosphorus nuclear magnetic resonance study. *Biochem. J.* **192**, 191–202 (1980).
6. Longley, R. W., Bortnick, R. J. and Roe, J. H. Rate of glycogenesis in liver of depancreatized rat after parenteral administration of glucose and fructose. *Proc. Soc. Exp. Biol. Med.* **94**, 108–110 (1957).
7. Youn, J. H., Youn, M. S. and Bergman, R. N. Synergism of glucose and fructose in net glycogen synthesis in perfused rat livers. *J. Biol. Chem.* **261**, 15960–15969 (1986).
8. Van den Berghe, G., Hue, L. and Hers, H.-G. Effect of administration of fructose on the glycogenolytic action of glucagon. An investigation of the pathogeny of hereditary fructose intolerance. *Biochem. J.* **134**, 637–645 (1973).
9. Thurston, J. H., Jones, E. M. and Hauhart, R. E. Failure of adrenaline to induce hyperglycaemia after fructose injection in young mice. *Biochem. J.* **148**, 149–151 (1975).
10. Taylor, W. M., Storlien, L. H. and Jenkins, A. B. Effect of fructose on phenylephrine-induced glucose output in perfused rat liver. *Horm. Metab. Res.* **20**, 528–530 (1988).
11. Nivelon, J.-L., Mathieu, M., Kissin, C., Collombel, C., Cotte, J. and Béthenod, M. Intolérance au fructose. Observation et mécanisme physiopathologique de l'hypoglucosémie. *Ann. Pédiatr.* **14**, 817–824 (1967).
12. Youn, J. H., Kaslow, H. R. and Bergman, R. N. Fructose effect to suppress hepatic glycogen degradation. *J. Biol. Chem.* **262**, 11470–11477 (1987).
13. Kaufmann, U. and Froesch, E. R. Inhibition of phosphorylase-*a* by fructose-1-phosphate, α-glycerophosphate and fructose-1,6-diphosphate: explanation for fructose-induced hypoglycemia in hereditary fructose intolerance and fructose-1,6-diphosphatase deficiency. *Eur. J. Clin. Invest.* **3**, 407–413 (1973).
14. Thurston, J. H., Jones, E. M. and Hauhart, R. E. Decrease and inhibition of liver glycogen phosphorylase after fructose. An experimental model for the study of hereditary fructose intolerance. *Diabetes* **23**, 597–604 (1974).
15. Iles, R. A., Stevens, A. N., Griffiths, J. R. and Morris, P. Phosphorylation status of liver by ^{31}P-NMR spectroscopy, and its implications for metabolic control. A comparison of ^{31}P-NMR spectroscopy (*in vivo* and *in vitro*) with chemical and enzymic determinations of ATP, ADP and P_i. *Biochem. J.* **229**, 141–151 (1985).
16. Malloy, C. R., Cunningham, C. C. and Radda, G. K. The metabolic state of the rat liver *in vivo* measured by ^{31}P-NMR spectroscopy. *Biochim. Biophys. Acta* **885**, 1–11 (1986).
17. Bar-Tana, J. and Cleland, W. W. Rabbit muscle phosphofructokinase. I. Anomeric specificity; initial velocity kinetics. *J. Biol. Chem.* **249**, 1263–1270 (1974).
18. Koerner, T. A. W. Jr., Younathan, E. S., Ashour, A.-L. E. and Voll, R. J. The fructose 6-phosphate site of phosphofructokinase. I. Tautomeric and anomeric specificity. *J. Biol. Chem.* **249**, 5749–5754 (1974).
19. Decanniere, C., Van Hecke, P., Vanstapel, F., Chen, H., Van Huffel, S., van der Voort, C., van Tongeren, B. and van Ormondt, D. Evaluation of signal processing methods for the quantification of strongly overlapping peaks in ^{31}P NMR spectra. *J. Magn. Reson. Ser. B* **105**, 31–37 (1994).
20. Rawson, N. E., Blum, H., Osbakken, M. D. and Friedman, M. I. (1994), Hepatic phosphate trapping, decreased ATP, and increased feeding after 2,5-anhydro-D-mannitol. *Am. J. Physiol.* **266**, R112–R117 (1977).
21. Raushel, F. M. and Cleland, W. W. Bovine liver fructokinase: purification and kinetic properties. *Biochemistry* **16**, 2169–2175 (1977).
22. Dills, W. L. Jr., Covey, T. R., Springer, P., Neal, S. and Rappaport, M. S. 2,5-Anhydro-l-deoxy-D-lyxitol, 2,5-anhydro-l-deoxy-D-mannitol, and 2,5-anhydro-l-deoxy-D-talitol. Synthesis and enzymic studies. *Carbohydr. Res.* **99**, 23–31 (1982).
23. Dills, W. L. Jr., Murphy-Kothe, J. and Klinger, J. Absorption, excretion and tissue distribution of 1-[^{3}H]-2,5-anhydro-D-mannitol in female Wistar rats. *Biochem. Arch.* **8**, 69–74 (1992).
24. Riquelme, P. T., Wernette-Hammond, M. E., Kneer, N. M. and Lardy, H. A. Mechanism of action of 2,5-anhydro-D-mannitol in hepatocytes. Effects of phosphorylated metabolites on enzymes of carbohydrate metabolism. *J. Biol. Chem.* **259**, 5115–5123 (1984).
25. Stevens, H. C. and Dills, W. I. Jr. Inhibition of glycogenolysis by 2,5-anhydro-D-mannitol in isolated rat hepatocytes. *FEBS Lett.* **165**, 247–250 (1984).
26. Stevens, H. C., Covey, T. R. and Dills, W. L. Jr. Inhibition of gluconeogenesis by 2,5-anhydro-D-mannitol in rat hepatocytes. *Biochim. Biophys. Acta* **845**, 502–506 (1985).
27. Hanson, R. L., Ho, R. S., Wiseberg, J. J., Simpson, R., Younathan, E. S. and Blair, J. B. Inhibition of gluconeogenesis and glycolysis by 2,5-anhydro-D-mannitol. *J. Biol. Chem.* **259**, 218–223 (1984).
28. Tordoff, M. G., Rafka, R., DiNovi, M. J. and Friedman, M. I. 2,5-

Anhydro-D-mannitol: a fructose analogue that increases food intake in rats. *Am. J. Physiol.* **254**, R150–R153 (1988).
29. Horton, D. and Philips, K. D. The nitrous acid deamination of glycosides and acetates of 2-amino-2-deoxy-D-glucose. *Carboh. Res.* **30**, 367–374 (1973).
30. Murphy, E. J., Bates, T. E., Williams, S. R., Watson, T., Brindle, K. M., Rajagopalan, B. and Radda, G. K. Endoplasmic reticulum: the major contributor to the PDE peak in hepatic ^{31}P-NMR spectra at low magnetic field strengths. *Biochim. Biophys. Acta* **1111**, 51–58 (1992).
31. Vanstapel, F., Waebens, M., Van Hecke, P., Decanniere, C. and Stalmans, W. The cytosolic concentration of phosphate determines the maximal rate of glycogenolysis in perfused rat liver. *Biochem. J.* **266**, 207–212 (1990).
32. Borgs, M., Van Hecke, P., Overloop, K., Decanniere, C., Van Huffel, S., Stalmans, W. and Vanstapel, F. *In situ* ^{13}C NMR quantification of hepatic glycogen. *NMR Biomed.* **6**, 371–376 (1993).
33. Vandebroeck, A., Bollen, M., De Wulf, H. and Stalmans, W. An assessment of the importance of intralysosomal and of α-amylolytic glycogenolysis in the liver of normal rats and of rats with a glycogen-storage disease. *Eur. J. Biochem.* **153**, 621–628 (1985).
34. Freeman, R. and Hill, H. D. W. Phase and intensity anomalies in Fourier transform NMR. *J. Magn. Reson.* **4**, 366–383 (1971).
35. Van Hecke, P., Decanniere, C. and Vanstapel, F. Double-tuned resonator designs for NMR spectroscopy. *J. Magn. Reson.* **84**, 170–176 (1989).
36. Cabañas, M. and van den Boogaart, A. Magnetic Resonance User Interface (MRUI) version 96.3 (1996). Available from http://www.mrui.uab.es.
37. van der Veen, J.W.C., de Beer, R., Luyten, P. R. and van Ormondt, D. Accurate quantitation of *in vivo* ^{31}P NMR signals using the variable projection method and prior knowledge. *Magn. Res. Med.* **6**, 92–98 (1988).
38. Brauer, M. and Sykes, B. D. Phosphorus-31 nuclear magnetic resonance studies of adenosine 5′-triphosphate bound to a nitrated derivative of G-actin. *Biochemistry* **20**, 6767–6775 (1981).
39. Gray, G. R. An examination of D-fructose 1,6-diphosphate and related sugar phosphates by Fourier transform ^{31}P nuclear magnetic resonance spectroscopy. *Biochemistry* **10**, 4705–4711 (1971).
40. Gard, J. K. and Ackerman, J. J. H. A [31]P NMR external reference for intact biological systems. *J. Magn. Reson.* **51**, 124–127 (1983).
41. Ernst, R. R. and Anderson, W. A. Application of Fourier transform spectroscopy to magnetic resonance. *Rev. Sci. Instrum.* **37**, 93–102 (1966).
42. Malloy, C. R., Cunningham, C. C. and Radda, G. K. The metabolic state of the rat liver *in vivo* measured by ^{31}P-NMR spectroscopy. *Biochim. Biophys. Acta* **885**, 1–11 (1986).
43. Fersht, A. Chapter 3. The basic equations of enzyme kinetics. In Enzyme Structure and Mechanism. pp. 84–102. Freeman, San Francisco, CA (1977).
44. Deming, W. E., Chapter IX. Systematic computations for fitting curves by least squares. In Statistical Adjustment of Data. pp. 148–171. Dover, New York (1964).
45. Van de Werve, G. and Hers, H.-G. Mechanism of activation of glycogen phosphorylase by fructose in the liver. Stimulation of phosphorylase kinase related to the concentration of adenosine triphosphate. *Biochem. J.* **178**, 119–126 (1979).
46. Vandebroeck, A., Uyttenhove, K., Bollen, M. and Stalmans, W. The hepatic glycogenolysis induced by reversible ischaemia or KCN is exclusively catalysed by phosphorylase A. *Biochem. J.* **256**, 685–688 (1988).
47. Hue, L. Role of fructose 2,6-bisphosphate in the stimulation of glycolysis by anoxia in isolated hepatocytes. *Biochem. J.* **206**, 359–365 (1982).
48. Riquelme, P. T., Kneer, N. M., Wernette-Hammond, M. E. and Lardy, H. A. Inhibition by 2,5-anhydromannitol of glycolysis in isolated rat hepatocytes and in Ehrlich ascites cells. *Proc. Natl Acad. Sci. USA* **82**, 78–82 (1985).
49. Stalmans, W. and Gevers, G. The catalytic activity of phosphorylase *b* in the liver. With a note on the assay in the glycogenolytic direction. *Biochem. J.* **200**, 327–336 (1981).
50. Stalmans, W., Bollen, M. and Mvumbi, L. Control of glycogen metabolism in health and disease. *Diab. Metab. Rev.* **3**, 127–161 (1987).
51. Stalmans, W., de Wulf, H., Hue, L. and Hers, H.-G. The sequential inactivation of glycogen phosphorylase and activation of glycogen synthase in liver after the administration of glucose to mice and rats. The mechanism of the hepatic treshold to glucose. *Eur. J. Biochem.* **41**, 127–134 (1974).
52. Shulman, G. I., Rothman, D. L., Chung, Y., Rossetti, L., Petit, W. A. Jr., Barrett, E. J. and Shulman, R. G. ^{13}C NMR studies of glycogen turnover in the perfused rat liver. *J. Biol. Chem.* **263**, 5027–5029 (1988).
53. Massillon, D., Bollen, M., De Wulf, H., Overloop, K., Vanstapel, F., Van Hecke, P. and Stalmans, W. Demonstration of a glycogen/glucose l-phosphate cycle in hepatocytes from fasted rats. Selective inactivation of phosphorylase by 2-deoxy,2-fluoro-α-D-glucopyranosyl fluoride. *J. Biol. Chem.* **270**, 19351–19356 (1995).
54. Ciudad, C. J., Massagué, J., Salavert, A. and Guinovart, J. J. Synthesis of glycogen from fructose in the presence of elevated levels of glycogen phosphorylase *a* in rat hepatocytes. *Mol. Cell. Biochem.* **30**, 33–38 (1980).
55. Parniak, M. A. and Kalant, N. Enhancement of glycogen concentrations in primary cultures of rat hepatocytes exposed to glucose and fructose. *Biochem. J.* **251**, 795–802 (1988).
56. Laughlin, M. R. and Barrett, E. J. Regulation of glycogen metabolism in liver by fructose infusion. Ninth Annual Scientific Meeting of the Society of Magnetic Resonance in Medicine, Abstracts, p. 940 (1990).

